Materials Performance and Characterization

doi:10.1520/MPC20220109 / Vol. 12 / No. 3 / 2023 / available online at www.astm.org

Fernanda Martins Queiroz,[1] Gleicy de Lima Xavier Ribeiro,[2] Renato Spacini de Castro,[2] Rogério Góes dos Santos,[2] Alexandre Vieira,[3,4] Maysa Terada,[2] Aline de Fátima Santos Bugarin,[2] Wagner de Rossi,[4] and Isolda Costa[4]

Study of the Effect of Nanosecond Laser Texturing on the Corrosion Behavior of Ti6Al4V and Ti6Al4V Parts Produced by Powder Bed Fusion

Reference

F. Martins Queiroz, G. L. X. Ribeiro, R. S. de Castro, R. G. dos Santos, A. Vieira, M. Terada, A. F. S. Bugarin, W. de Rossi, and I. Costa, "Study of the Effect of Nanosecond Laser Texturing on the Corrosion Behavior of Ti6Al4V and Ti6Al4V Parts Produced by Powder Bed Fusion," *Materials Performance and Characterization* 12, no. 3 (2023): 341–350. https://doi.org/10.1520/MPC20220109

ABSTRACT

Combining metallic additive manufacturing with laser texturing could be an alternative in obtaining parts with functional hydrophilic surfaces, which improves osteointegration. Careful study of the corrosion behavior of the surfaces obtained is necessary, because the evolution of this phenomenon can influence the osteointegration of the implant, causing the release of metal ions in the body and even the rejection of the component. This study compared the corrosion behavior of laser texturing Ti6Al4V components with components manufactured using laser power bed fusion of the same alloy followed by laser texturing. Their microstructure, roughness, wettability, and electrochemical behavior were analyzed, and different morphologies and microtopographies were observed comparing both samples. The electrochemical tests obtained indicate that Ti6Al4V showed higher corrosion resistance than L-PBF Ti6Al4V after laser texturing. The results suggest that laser texturing can encourage cell proliferation and osseointegration on the surface of Ti6Al4V biomedical implants.

Keywords

laser texturing, additive manufacturing, Ti6Al4V

Manuscript received November 25, 2022; accepted for publication March 3, 2023; published online September 1, 2023. Issue published December 18, 2023.

[1] Faculdade SENAI São Paulo Campus Suíço-Brasileira "Paulo Ernesto Tolle" - Santo Amaro, Bento Branco de Andrade Filho, 379, São Paulo, São Paulo 04757-000, Brazil (Corresponding author), e-mail: mq_fernanda@yahoo.com.br, https://orcid.org/0000-0003-3309-1116

[2] SENAI Innovation Institute for Advanced Manufacturing and Microfabrication, Bento Branco de Andrade Filho, São Paulo, São Paulo 04757-000, Brazil, https://orcid.org/0000-0001-5400-7513 (G.L.X.R.), https://orcid.org/0000-0002-8707-3004 (R.G.S.), https://orcid.org/0000-0002-2011-5759 (M.T.), https://orcid.org/0000-0002-0386-8142 (A.F.S.B.)

[3] Faculdade SENAI São Paulo Campus Suíço-Brasileira "Paulo Ernesto Tolle" - Santo Amaro, Bento Branco de Andrade Filho, 379, São Paulo, São Paulo 04757-000, Brazil, https://orcid.org/0000-0002-9969-9709

[4] Institute of Energy and Nuclear Research, Av Lineu Prestes, 2242, São Paulo, São Paulo 05508-000, Brazil, https://orcid.org/0000-0003-1371-7521 (W.R.), https://orcid.org/0000-0002-4987-3334 (I.C.)

Introduction

Titanium Ti-6Al-4V alloy (ISO 5832-2, *Implants for Surgery—Metallic Materials—Part 2: Unalloyed Titanium*) is the widely used titanium-based alloy in biomedical applications because of its unique properties, including higher corrosion resistance, elastic modulus similar to the bone and high mechanical strength-to-weight ratio in comparison with stainless steels and CoCrMo alloys.[1]

Additive manufacturing is a 3-D printing process focusing on complex geometries, lighter parts, and customized products, making it an ideal technique to produce implants.[1] The reduction of mismatch between natural bone and implant promotes faster recovery. Besides, laser power bed fusion (L-PBF) additive manufactured implants also can incorporate porous and solid components into one block, facilitating the osseointegration process.[2] It is valid to consider the possibility of creating a 3-D structure based on research conducted in anodized titanium alloys, aiming at increasing the area combined with textures or geometries or both.[3] Many TiAlV ideal additive manufacturing parameters can be found in the literature, including the chamber conditions, such as build plate temperature, ambient temperature, pressure oxygen concentration; laser power, speed scan, melt-pool status, powder layer distribution on the build surface, etc. However, these parameters cannot be considered as well established, as they depend not only on the laser type and power but also on the powder characteristics.

Presently, most commercial orthopedics implants are manufactured by subtractive manufacturing, and their functional surface is made by ceramic coating, such as hydroxyapatite, or polymeric materials, trying to improve not only the corrosion resistance but also the osseointegration process. However, these layers can suffer detachment, residual stress, and cracks during their process, favoring localized corrosion of the metallic implant. The process of anodizing in titanium alloys also has advantages in increasing osseointegration, because the number of cells adhered to titanium dioxide (TiO_2) nanotubes increases significantly by 300–400 % compared with cells that adhere to the surface of the titanium metal, which can be explained by the topological characteristics and increase in the surface area.[4] However, it is still a challenge to manufacture a plain and environmentally friendly coating that is durable and corrosion resistant.

Surface texturing has developed in the last decade as a viable option for coating, resulting in significant improvements in load capacity, wear resistance, friction coefficient of mechanical components, and corrosion resistance. Several techniques can be employed for surface texturing, but the use of laser is probably the most advanced. The use of femtosecond and picosecond laser texturing shows excellent results increasing the corrosion resistance of metal alloys. Besides, the geometric resolution and the characteristics of the microstructure produced by their laser beam is much more accurate than the nanosecond one. However, the high cost of both femto and picosecond lasers discourages their use at industrial production. Thus, the nanosecond laser texturing has been studied, associated or not, with chemical treatments.[5–14]

The laser focuses on the surface producing a large number of microcavities, and each of these microstructures acts as a hydrodynamic bearing, microdeposit for air, lubricant, or even debris, contributing to mechanical sealing; piston rings; and axial bearings, in addition to changing surface properties such as corrosion resistance and wettability.[5–9,15] This last property allows for the reduction of bacterial adhesion to the surface of the implant, diminishing the patient's recovery time and avoiding the need for new surgeries caused by infections.[16,17] Besides, publications also have shown that microporosity is an essential

element in the osteoinduction of biomaterials as its architecture (pore shape and size) promotes bone formation as well as facilitates the exchange of nutritional components and oxygen to increase bone growth.[3] Based on the literature related to surfaces that aim to promote osseointegration, it is also found that the topological characteristic and increase in the surface area favor this process.[4,18–20] Components for orthopedic implants would have an average pore size ranging from 400 to 600 mm, representing a volume of 75–85 %.[21]

The surface wettability also favors protein adsorption, cell propagation, and cell fixation. Cell propagation and growth occur on hydrophilic surfaces because they promote extracellular matrix deposition and fixation by means of adhering molecules tied to intracellular actin filaments.[22] The contact angle measurement can be used to evaluate the wettability of a material, because the topology significantly influences the surface's ability to interact with the liquid, affecting the wettability of the surface.[13,14,23,24] To be considered hydrophobic, a surface must present a contact angle with water between 90° and 150°. Below 90°, the surface is hydrophilic and above 150°, superhydrophobic.[25]

The present study aims to evaluate the surface obtained in a laser-textured L-PBF additive-manufactured Ti6Al4V alloy. The microstructure, roughness, wettability, and electrochemical behavior were analyzed, as were different morphologies and microtopographies. These results indicate if these samples can encourage cell proliferation and osseointegration on the surface of Ti6Al4V biomedical implants. These characteristics influence the quality of life of patients, because they diminish not only the time of healing process but also the possibility of implant failure and consequent need for further surgery.

Materials and Methods

Ti6Al4V specimens were produced by additive manufacturing L-PBF using a speed scan of 100 mm/s, laser power of 244 W, hatch spacing of 0.07 mm, and slice thickness of 30 μm, using an Ytterbium laser with maximum beam power of 500 W. The scanning strategy was set with an alternating angle between layers of 67°. The process was performed in a controlled atmosphere with argon gas to minimize oxygen pick-up to <0.1 %. The equipment used to produce these specimens was an Omnitek 600, from Omnitek. Samples of 15 ×20 mm taken from a conventional sheet processed Ti6Al4V were also tested in this work, for comparison.

Samples of 1.0 cm^2 of Ti6Al4V were prepared by grinding with silicon carbide paper up to #600 and then washed with isopropanol. L-PBF Ti6Al4V samples were textured in as-built condition. The surfaces of these samples were textured using an ytterbium optical fiber laser, with a wavelength of 1,064 nm (infrared), nominal power of 50 W, pulse duration of 150 ns, laser speed of 35 mm/s, frequency of 2.0 kHz, focal length of 254 mm, and theoretical diameter of the beam at order of 70 μm. The texturing was performed in four passes using a P1000U GF laser texturing machine. The parameters were selected from previous works.[26] At least three samples of each condition were produced and evaluated. The results are highly reproducible as the laser texturing is a very accurate technique ($\Delta < 2$ %)[26–28] according to the predetermined parameters (power, number of passes, and frequency). and the diameter of the laser beam is around 70 μm.

All specimens were characterized using a scanning electron microscope (SEM) Hitachi TM3000, and their surface wettability was evaluated by a sessile drop contact angle method, before and after laser texturing, using a drop shape analyzer Kruss. Samples were placed on the bottom flat surface, and a droplet of deionized water (7–10 μL) was dropped into the center of the top surface at room temperature.

The roughness and topography of these specimens was measured using a laser confocal microscope Olympus LEXT OLS4100 evaluating the 3-D surface and the homogeneity as well as the reproducibility of the textures. The measured area was 6.25 mm^2, using a cutoff of 0.8 mm, because of the size of the samples. The surface was filtered using the Gaussian filter.

A Gamry PCI4/300 potentiostat-frequency response analyzer system was used to evaluate the corrosion resistance of the specimens. Electrochemical impedance spectroscopy (EIS) was carried out after the stabilization of the open circuit potential, in a classical three-electrode arrangement using 1.00 cm^2 area of the specimen as working electrode, Ag/AgCl (silver metal and silver chloride solution) (+0.197 V versus standard hydrogen electrode [SHE]) as reference electrode, and a platinum plate as counter electrode. EIS measurements were taken at

TABLE 1
PBS

Reagent	Amount, g/L
NaCl	8.50
Na_2HPO_4	1.55
$Na2H_2PO_4$	0.23

different immersion times at room temperature, in a naturally aerated phosphate buffered solution (PBS)[29,30] at pH = 3.0 (Table 1), over a frequency range from 10^5 to 10^{-2} Hz with 10 points per decade using an AC signal amplitude of 10 mV (rms). Tests were performed up to 48 h. All electrochemical tests were performed in at least in triplicate, in order to ensure the reproducibility of the results.

The confocal microscope is located at the Universidade Federal do ABC. The other equipment is located at the SENAI Innovation Institute for Advanced Manufacturing and Microfabrication.

Results and Discussion

Figure 1 shows the micrography of both Ti6Al4V and L-PBF Ti6Al4V samples. Figure 1*A* shows the ground surface of the Ti4Al6V sample, and figure 1*B* presents the as-built L-PBF Ti6Al4V sample, with pores and spherical partially melted powder particles, characteristic of L-PBF process, in agreement with the literature.[31] Figure 2 shows both samples after texturing: the surface of the Ti4Al6V sample presented microgrooves and microdimples, creating a regular pattern, as expected [26,27] (fig. 2*A* and 2*C*). On the other hand, the surface of the L-PBF Ti6Al4V was flattened, in comparison with as-built surface, presenting microgrooves. Despite the presence of pores caused from the printing process, the unmelted powder was not detected any longer (fig. 2*B* and 2*D*).

Figure 3 shows the 3-D topography of all samples. Figure 3*A* and 3*B* presents the reference surface of both Ti6Al4V (ground up to 600#) and L-PBF Ti6Al4V (as-built condition), respectively. The L-PBF samples were not ground prior to the laser texturing in order to evaluate the effect of this technique in the unprocessed surface. Figure 3*C* and 3*D* shows that multioriented structures are generated from the constant melting, ablation, and material deposition during the process, similar to the textures reported in the literature.[26,32] The laser texturing increased the surface roughness of both materials. However, the ground surface became more homogeneous, favoring the reproducibility of commercial component manufacturing. The L-PBF Ti6Al4V samples presented a similar range of roughness before and after the laser texturing.

FIG. 1 Surface characterization of (*A*) Ti6Al4V and (*B*) L-PBF Ti6Al4V. SEM images, BSE detector.

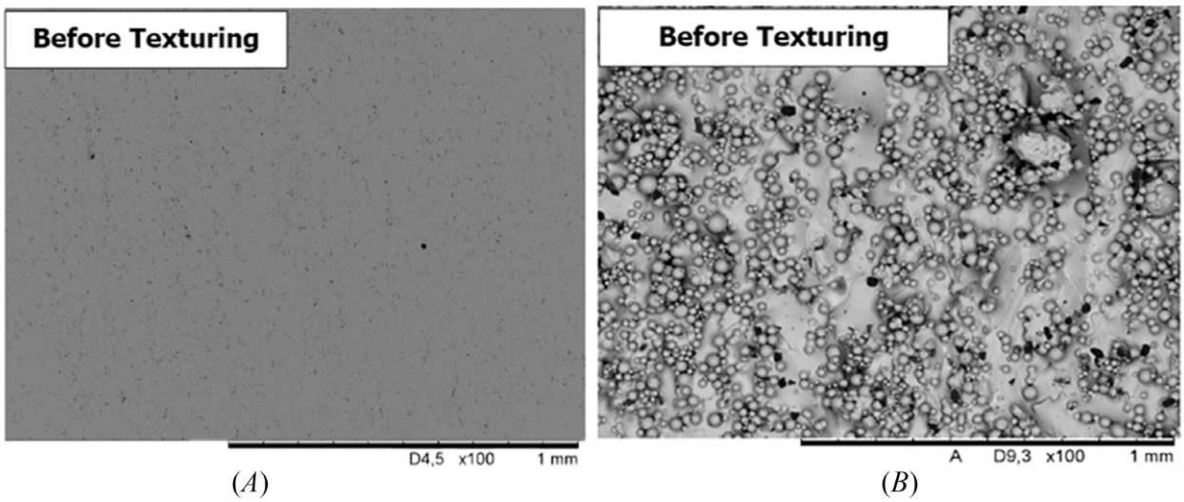

FIG. 2 Surface characterization of samples Ti6Al4V after LASER texturing. (*A*) Ti6Al4V and (*B*) L-PBF Ti6Al4V, (*C*) and (*D*) same at higher magnifications. SEM images, BSE detector.

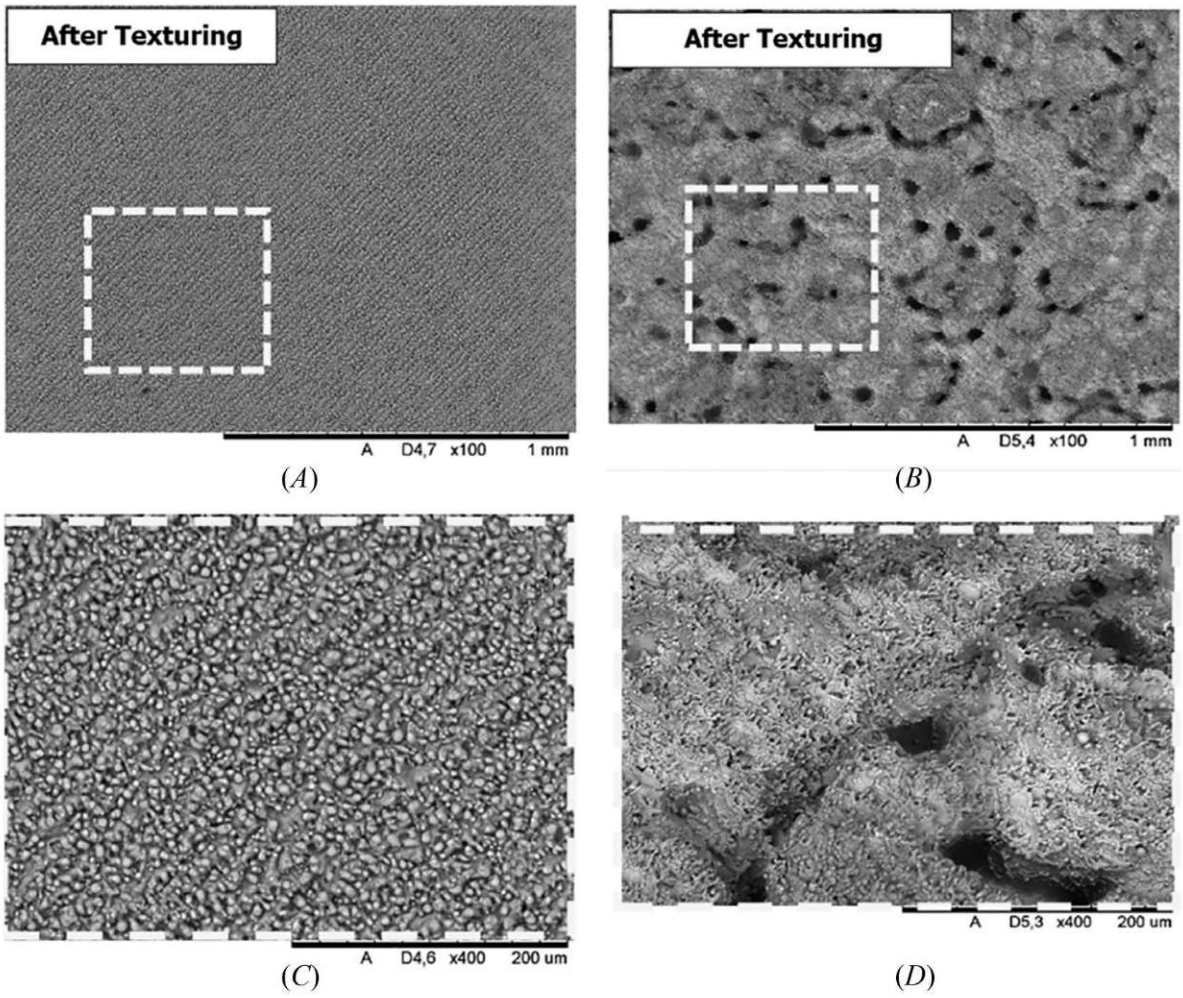

The quantitative roughness of all surfaces was evaluated, and results are presented in **Table 2**, showing not only both the 3-D average roughness (Sa) and maximum peak-to-valley height of the profile (Sz) surface roughness parameters but also the skewness or asymmetry of the profile about the mean line (Ssk) and the kurtosis or "tailedness" of the profile about the mean line (Sku), permitting a greater understanding of surface morphology.

The average roughness (Sa) of Ti6Al4V laser-textured samples is around 2 μm, one order of magnitude lower than the L-PBF Ti6Al4V laser-textured samples. This result was expected as the as-built samples presented unmelted particles and pores on their surfaces (**fig. 3*B***). Therefore, the Ti6Al4V results suggest that laser texturing can benefit the cell proliferation and osseointegration on the surface of biomedical implants, as literature reports that Ra values below 5 μm are the best condition for this process.[19,33–36] Moreover, literature also reports that osteoblasts were more likely to attach to pronounced micro-nanostructure surfaces than those with a higher degree of wettability.[37] Besides, both Sz maximum values were one order of magnitude higher than their Sa, also in agreement with the literature.[26] It was attributed to the laser texture concept on samples surfaces.

The Sku parameter showed that all Ti6Al4V samples presented a flat height distribution (Rku < 4).[38] On the other hand, the Ssk negative value of the L-PBF Ti6Al4V laser-textured samples can be explained by high proportion of deep valleys in the sample, in comparison with the number of high peaks, confirming the reduction of partially melted powder particles on the surface.

FIG. 3 The 3-D surface topography of both samples: (*A*) Ti6Al4V, (*B*) Ti6Al4V laser textured, (*C*) L-PBF Ti6Al4V, and (*D*) L-PBF Ti6Al4V laser textured. Laser confocal microscope.

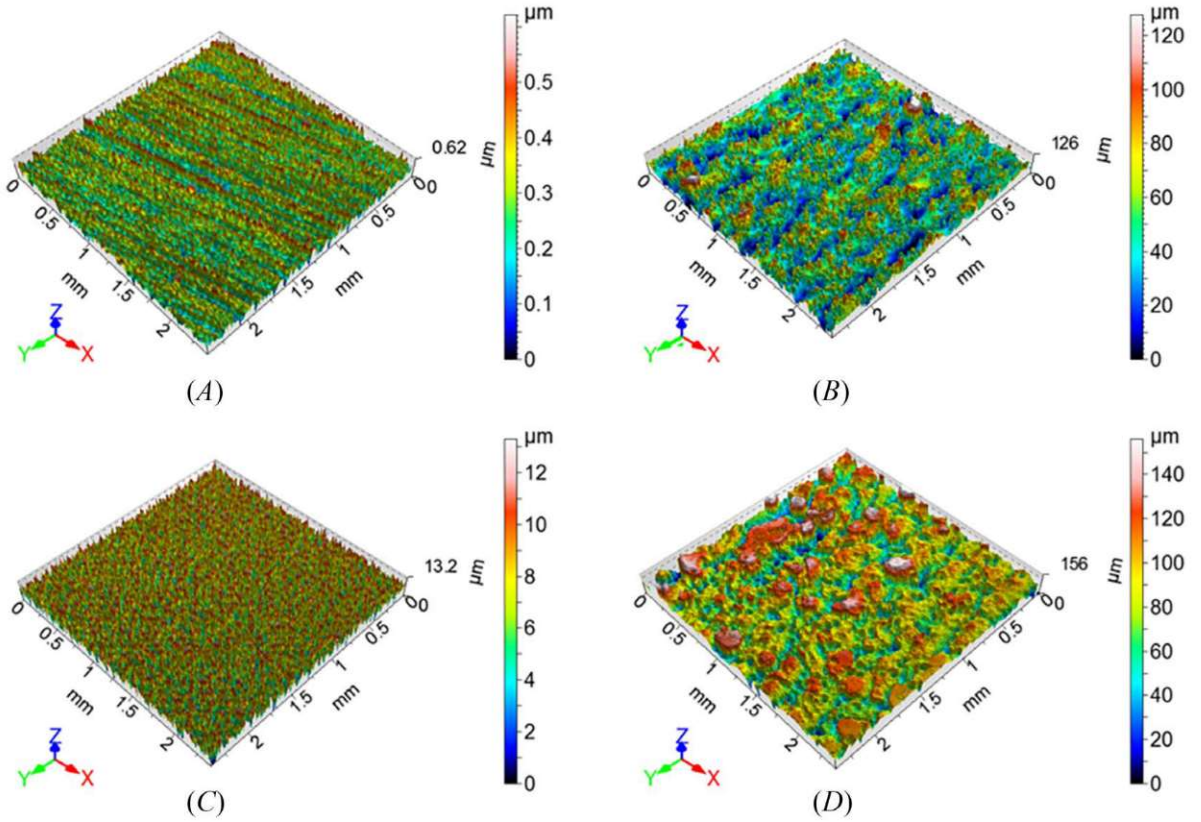

TABLE 2
Roughness measurements of both Ti6Al4V and L-PBF Ti6Al4V: Sa, Sz, Sku, and Ssk parameters, determined from **figure 3**

Sample	Sa, µm	Sz, µm	Sku, µm	Ssk, µm
Ti6Al4V	0.09	0.62	2.98	0.04
Ti6Al4V laser textured	2.11	13.30	2.73	0.13
L-PBF Ti6Al4V	16.26	127.70	3.31	0.32
L-PBF Ti6Al4V laser textured	23.25	156.07	3.14	−0.40

TABLE 3
Contact angle of L-PBF Ti6Al4V or Ti6Al4V samples before and after laser texturing

Sample	Contact Angle, °
Ti6Al4V	124.76 ± 1.39
Ti6Al4V laser textured	[a]
L-PBF Ti6Al4V	59.64 ± 3.75
L-PBF Ti6Al4V laser textured	53.96 ± 0.76

Note: [a] Measurement could not be performed as the drop spread immediately after reaching the surface.

The influence of the surface roughness in the wettability of both materials was determined using a drop shape analyzer. **Table 3** presents contact angle measurements of both L-PBF Ti6Al4V and Ti6Al4V samples determined by a sessile drop method, before and after laser texturing. Before laser texturing, Ti6Al4V samples were

FIG. 4 EIS results for the L-PBF Ti6Al4V and Ti6Al4V after laser texturing as a function of exposure time in PBS solution. (*A*) Nyquist and (*B*) Bode phase angle.

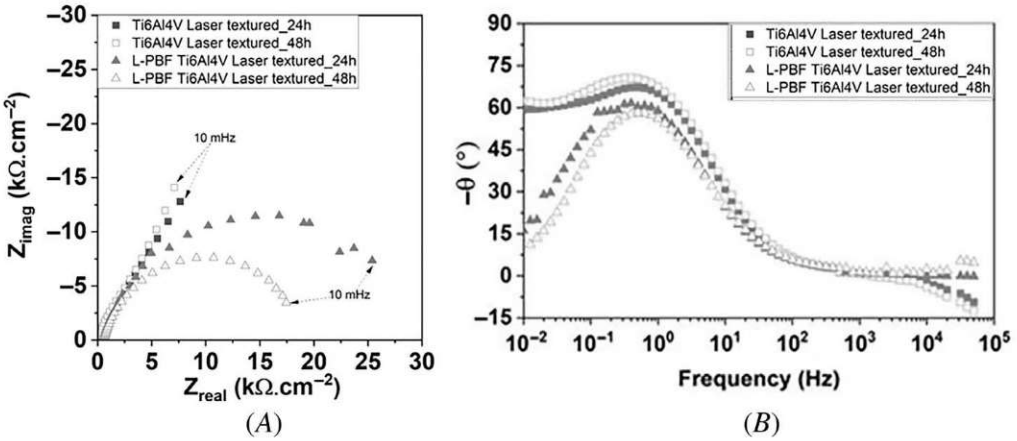

FIG. 5 SEM images after EIS tests. (*A*) Ti6Al4V laser textured, (*B*) same at higher magnifications, (*C*) L-PBF Ti6Al4V laser textured, and (*D*) same at higher magnifications. After 48 h of immersion in PBS. BSE detector.

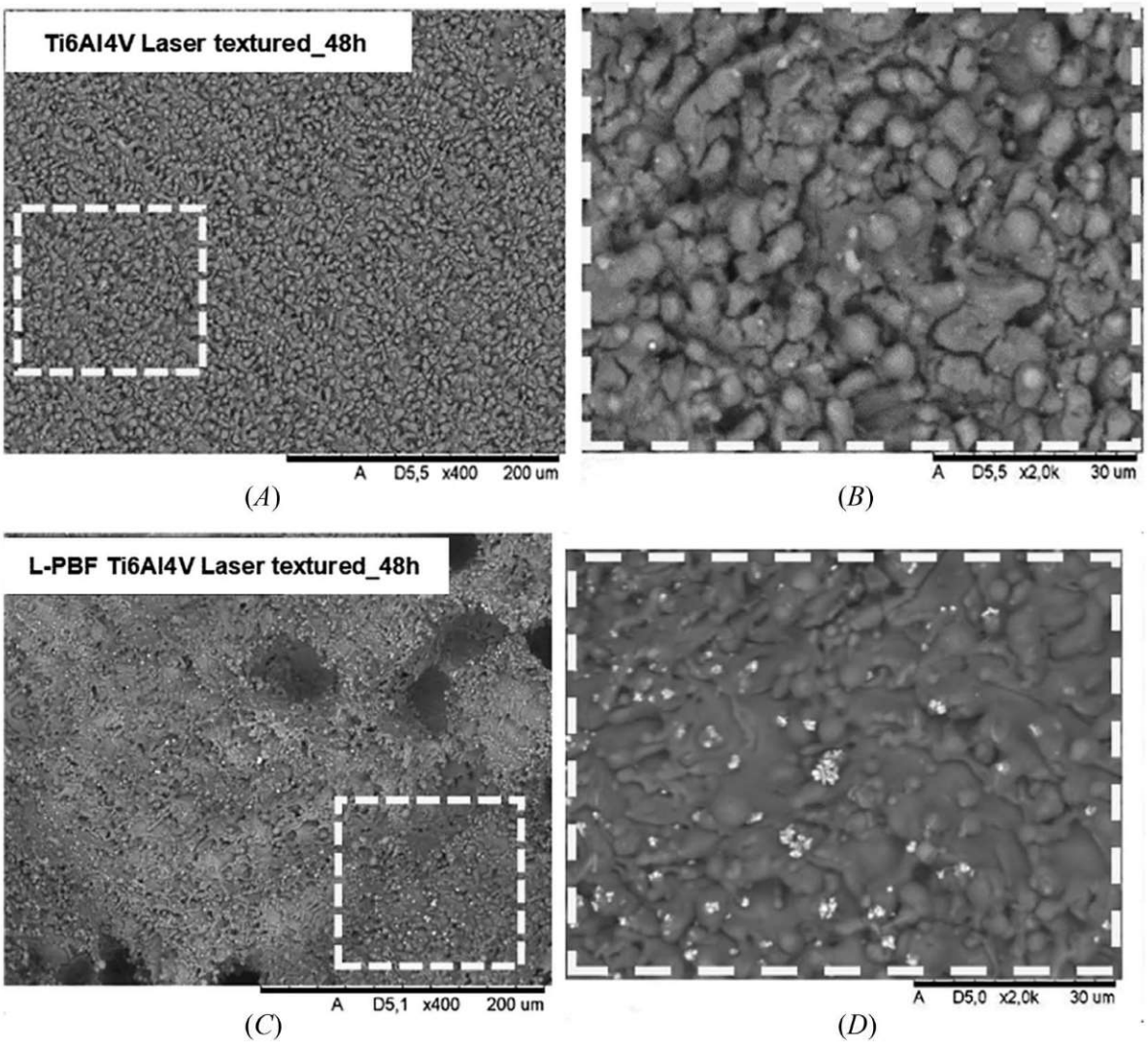

hydrophobic, and the L-PBF Ti6Al4V samples were hydrophilic. However, the laser texturing process turned both samples hydrophilic. These results can be explained by the micro- and nano-microstructure generated by the laser texturing.

The corrosion resistance of all samples was also evaluated, and **figure 4** presents EIS results for the L-PBF Ti6Al4V and Ti6Al4V after laser texturing as a function of exposure time in the PBS solution. The EIS results present the surface characteristics of the sample, estimating the presence and quantity of defects and the degradation of properties with immersion time. The impedance modulus values at 0.01 Hz were of the order of 10^4 $\Omega.cm^2$ for both samples with higher impedances associated to the Ti6Al4V samples. After 48 h of tests, the impedance values of the L-PBF Ti6Al4V samples diminish in comparison with the EIS results obtained after 24 h (**fig. 4*A***). However, both values remained similar for the Ti6Al4V samples. Moreover, Ti6Al4V Bode phase diagrams presented two time constants being the first peak approximately at 1 Hz. The peak at medium frequencies is associated to the charge transfer on the surface and the peak at lower frequencies, to the oxide layer (**fig. 4*B***). On the other hand, L-PBF Ti6Al4V samples presented only one peak at medium frequencies, indicating their lower corrosion resistance. These results are according to the literature[39] and can be explained by the microstructural difference between the samples. The L-PBF Ti6Al4V is predominantly α', whereas the Ti6Al4V has an α + β dual phase.[40,41]

The surface of all samples was observed using SEM, after the electrochemical tests (**fig. 5*)***. Micrographs show that it was not possible to find localized corrosion on both L-PBF Ti6Al4V and Ti6Al4V samples after EIS tests.

Conclusions

This study presents laser texturing of L-PBF Ti6Al4V and Ti6Al4V specimens. Their microstructure, roughness, wettability, and electrochemical behavior were analyzed, and different morphologies and microtopographies were observed comparing both samples.

The laser texturing produced periodic micropatterns on the Ti6Al4V and flattened the L-PBF Ti6Al4V surface, removing unmelted powder from the surface. Besides, both Ti6Al4V and L-PBF Ti6Al4V samples were hydrophilic after this process.

Ti6Al4V showed higher corrosion resistance than L-PBF Ti6Al4V after laser texturing after 24 h and 48 h of immersion in PBS solution.

The results suggest that laser texturing can encourage cell proliferation and osseointegration on the surface of Ti6Al4V biomedical implants. These results are very encouraging to diminish the healing process of patients.

References

1. K. C. Wong and P. Scheinemann, "Additive Manufactured Metallic Implants for Orthopaedic Applications," *Science China Materials* 61, no. 4 (April 2018): 440–454, https://doi.org/10.1007/s40843-017-9243-9
2. R. A. García-León, J. A. Gómez-Camperos, and H. Y. Jaramillo, "Scientometric Review of Trends on the Mechanical Properties of Additive Manufacturing and 3D Printing," *Journal of Materials Engineering and Performance* 30, no. 7 (July 2021): 4724–4734, https://doi.org/10.1007/s11665-021-05524-7
3. S. Arabnejad, R. Burnett Johnston, J. A. Pura, B. Singh, M. Tanzer, and D. Pasini, "High-Strength Porous Biomaterials for Bone Replacement: A Strategy to Assess the Interplay between Cell Morphology, Mechanical Properties, Bone Ingrowth and Manufacturing Constraints," *Acta Biomaterialia* 30 (January 2016): 345–356, https://doi.org/10.1016/j.actbio.2015.10.048
4. S. Oh, C. Daraio, L.-H. Chen, T. R. Pisanic, R. R. Fiñones, and S. Jin, "Significantly Accelerated Osteoblast Cell Growth on Aligned TiO_2 Nanotubes," *Journal of Biomedical Materials Research. Part A* 78A, no. 1 (July 2006): 97–103, https://doi.org/10.1002/jbm.a.30722
5. J. I. Ahuir-Torres, M. A. Arenas, W. Perrie, G. Dearden, and J. de Damborenea, "Surface Texturing of Aluminium Alloy AA2024-T3 by Picosecond Laser: Effect on Wettability and Corrosion Properties," *Surface and Coatings Technology* 321 (2017): 279–291, https://doi.org/10.1016/j.surfcoat.2017.04.056
6. Y. Cai, W. Chang, X. Luo, A. M. L. Sousa, K. H. A. Lau, and Y. Qin, "Superhydrophobic Structures on 316L Stainless Steel Surfaces Machined by Nanosecond Pulsed Laser," *Precision Engineering* 52 (2018): 266–275, https://doi.org/10.1016/j.precisioneng.2018.01.004

7. B. Dashtbozorg, X. Li, J.-M. Romano, A. Garcia-Giron, R. L. Sammons, S. Dimov, and H. Dong, "A Study on the Effect of Ultrashort Pulsed Laser Texturing on the Microstructure and Properties of Metastable S Phase Layer Formed on AISI 316L Surfaces," *Applied Surface Science* 511 (2020): 145557, https://doi.org/10.1016/j.apsusc.2020.145557
8. A. He, W. Liu, W. Xue, H. Yang, and Y. Cao, "Nanosecond Laser Ablated Copper Superhydrophobic Surface with Tunable Ultrahigh Adhesion and Its Renewability with Low Temperature Annealing," *Applied Surface Science* 434 (2018): 120–125, https://doi.org/10.1016/j.apsusc.2017.10.143
9. L. M. Vilhena, M. Sedlaček, B. Podgornik, J. Vižintin, A. Babnik, and J. Možina, "Surface Texturing by Pulsed Nd:YAG Laser," *Tribology International* 42, no. 10 (October 2009): 1496–1504, https://doi.org/10.1016/j.triboint.2009.06.003
10. M. Zupančič, M. Može, P. Gregorčič, and I. Golobič, "Nanosecond Laser Texturing of Uniformly and Non-uniformly Wettable Micro Structured Metal Surfaces for Enhanced Boiling Heat Transfer," *Applied Surface Science* 399 (2017): 480–490, https://doi.org/10.1016/j.apsusc.2016.12.120
11. L. Boinovich and A. Emelyanenko, "A Wetting Experiment as a Tool to Study the Physicochemical Processes Accompanying the Contact of Hydrophobic and Superhydrophobic Materials with Aqueous Media," *Advances in Colloid and Interface Science* 179-182 (2012): 133–141, https://doi.org/10.1016/j.cis.2012.06.010
12. D.-M. Chun, C.-V. Ngo, and K.-M. Lee, "Fast Fabrication of Superhydrophobic Metallic Surface Using Nanosecond Laser Texturing and Low-Temperature Annealing," *CIRP Annals* 65, no. 1 (2016): 519–522, https://doi.org/10.1016/j.cirp.2016.04.019
13. D. Ta, A. Dunn, T. J. Wasley, R. W. Kay, J. Stringer, P. J. Smith, C. Connaughton, and J. D. Shephard, "Nanosecond Laser Txtured Superhydrophobic Metallic Surfaces and Their Chemical Sensing Applications," *Applied Surface Science* 357, Part A (December 2015): 248–254, https://doi.org/10.1016/j.apsusc.2015.09.027
14. U. Trdan, M. Hočevar, and P. Gregorčič, "Transition from Superhydrophilic to Superhydrophobic State of Laser Textured Stainless Steel Surface and Its Effect on Corrosion Resistance," *Corrosion Science* 123 (2017): 21–26, https://doi.org/10.1016/j.corsci.2017.04.005
15. Y. Cai, X. Luo, M. Maclean, Y. Qin, M. Duxbury, and F. Ding, "A Single-Step Fabrication Approach for Development of Antimicrobial Surfaces," *Journal of Materials Processing Technology* 271 (2019): 249–260, https://doi.org/10.1016/j.jmatprotec.2019.04.012
16. C. N. Elias, Y. Oshida, J. H. C. Lima, and C. A. Muller, "Relationship between Surface Properties (Roughness, Wettability and Morphology) of Titanium and Dental Implant Removal Torque," *Journal of the Mechanical Behavior of Biomedical Materials* 1, no. 3 (July 2008): 234–242, https://doi.org/10.1016/j.jmbbm.2007.12.002
17. A. Cunha, A.-M. Elie, L. Plawinski, A. P. Serro, A. M. Botelho do Rego, A. Almeida, M. C. Urdaci, M.-C. Durrieu, and R. Vilar, "Femtosecond Laser Surface Texturing of Titanium as a Method to Reduce the Adhesion of *Staphylococcus aureus* and Biofilm Formation," *Applied Surface Science* 360, Part B (January 2016): 485–493, https://doi.org/10.1016/j.apsusc.2015.10.102
18. J. Čapek, M. Machová, M. Fousová, J. Kubásek, D. Vojtěch, J. Fojt, E. Jablonská, J. Lipov, and T. Ruml, "Highly Porous, Low Elastic Modulus 316L Stainless Steel Scaffold Prepared by Selective Laser Melting," *Materials Science and Engineering: C* 69 (2016): 631–639, https://doi.org/10.1016/j.msec.2016.07.027
19. D. J. Cohen, A. Cheng, K. Sahingur, R. M. Clohessy, L. B. Hopkins, B. D. Boyan, and Z. Schwartz, "Performance of Laser Sintered Ti-6Al-4V Implants with Bone-Inspired Porosity and Micro/nanoscale Surface Roughness in the Rabbit Femur," *Biomedical Materials* 12, no. 2 (April 2017): 025021, https://doi.org/10.1088/1748-605X/aa6810
20. H. Liang, Y. Yang, D. Xie, L. Li, N. Mao, C. Wang, Z. Tian, Q. Jiang, and L. Shen, "Trabecular-Like Ti-6Al-4V Scaffolds for Orthopedic: Fabrication by Selective Laser Melting and In Vitro Biocompatibility," *Journal of Materials Science and Technology* 35, no. 7 (July 2019): 1284–1297, https://doi.org/10.1016/j.jmst.2019.01.012
21. B. R. Levine, S. Sporer, R. A. Poggie, C. J. Della Valle, and J. J. Jacobs, "Experimental and Clinical Performance of Porous Tantalum in Orthopedic Surgery," *Biomaterials* 27, no. 27 (September 2006): 4671–4681, https://doi.org/10.1016/j.biomaterials.2006.04.041
22. M. J. K. Lodhi, K. M. Deen, M. C. Greenlee-Wacker, and W. Haider, "Additively Manufactured 316L Stainless Steel with Improved Corrosion Resistance and Biological Response for Biomedical Applications," *Additive Manufacturing* 27 (2019): 8–19, https://doi.org/10.1016/j.addma.2019.02.005
23. R. N. Wenzel, "Resistance of Solid Surfaces to Wetting by Water," *Industrial & Engineering Chemistry* 28, no. 8 (August 1936): 988–994, https://doi.org/10.1021/ie50320a024
24. H. Yan, M. R. B. Abdul Rashid, S. Y. Khew, F. Li, and M. Hong, "Wettability Transition of Laser Textured Brass Surfaces inside Different Mediums," *Applied Surface Science* 427, Part B (January 2018): 369–375, https://doi.org/10.1016/j.apsusc.2017.08.218
25. A. M. Kietzig, S. G. Hatzikiriakos, and P. Englezos, "Patterned Superhydrophobic Metallic Surfaces," *Langmuir* 25, no. 8 (April 2009): 4821–4827, https://doi.org/10.1021/la8037582
26. R. G. dos Santos, "Influência de parâmetros do laser pulsado de itérbio na modificação de superfícies da liga Ti-6Al-4V" (masters thesis, Universidade de São Paulo, 2022).
27. GF Machining Solution, "Laser Process: C7 Tecnologia de Funcionamento," Technical Manual, 2017.
28. M. J. Coathup, G. W. Blunn, N. Mirhosseini, K. Erskine, Z. Liu, D. R. Garrod, and L. Li, "Controlled Laser Texturing of Titanium Results in Reliable Osteointegration," *Journal of Orthopaedic Research* 35, no. 4 (April 2017): 820–828, https://doi.org/10.1002/jor.23340

29. J. Pan, C. Karlén, and C. Ulfvin, "Electrochemical Study of Resistance to Localized Corrosion of Stainless Steels for Biomaterial Applications," *Journal of The Electrochemical Society* 147, no. 3 (February 2000): 1021, https://doi.org/10.1149/1.1393307
30. L. O. Berbel, "Avaliação da resistência à corrosão da liga Ti-6Al-4V para implantes dentários em ambientes aerados e deaerados" (PhD diss., Universidade de São Paulo, 2021).
31. N. K. Tolochko, S. E. Mozzharov, I. A. Yadroitsev, T. Laoui, L. Froyen, V. I. Titov, and M. B. Ignatiev, "Balling Processes during Selective Laser Treatment of Powders," *Rapid Prototyping Journal* 10, no. 2 (2004): 78–87, https://doi.org/10.1108/13552540410526953
32. M. S. F. de Lima and I. Almeida, "Surface Modification of Ti6Al4V Alloy by Pulsed Lasers: Microstructure and Hydrophobic Behavior," *Materials Research* 20, no. 1 (2017): 8–14, https://doi.org/10.1590/1980-5373-mr-2017-0221
33. M. K. Ibrahim, E. Hamzah, and S. N. Saud, "Microstructure, Phase Transformation, Mechanical Behavior, Bio-corrosion and Antibacterial Properties of Ti-Nb-xSn (x = 0, 0.25, 0.5 and 1.5) SMAs," *Journal of Materials Engineering and Performance* 28, no. 1 (January 2019): 382–393, https://doi.org/10.1007/s11665-018-3776-x
34. P. T. M. Le, S. A. Shintani, H. Takadama, M. Ito, T. Kakutani, H. Kitagaki, S. Terauchi, et al., "Bioactivation Treatment with Mixed Acid and Heat on Titanium Implants Fabricated by Selective Laser Melting Enhances Preosteoblast Cell Differentiation," *Nanomaterials* 11, no. 4 (April 2021): 987, https://doi.org/10.3390/nano11040987
35. H. M. Hamza, K. M. Deen, and W. Haider, "Microstructural Examination and Corrosion Behavior of Selective Laser Melted and Conventionally Manufactured Ti6Al4V for Dental Applications," *Materials Science and Engineering: C* 113 (2020): 110980, https://doi.org/10.1016/j.msec.2020.110980
36. C. Wu, M. Chen, T. Zheng, and X. Yang, "Effect of Surface Roughness on the Initial Response of MC3T3-E1 Cells Cultured on Polished Titanium Alloy," *Bio-medical Materials and Engineering* 26, no. s1 (2015): S155–S164, https://doi.org/10.3233/BME-151301
37. Y. O. Kravchenko, I. E. Garkusha, A. V. Taran, E. Coy, I. Iatsunskyi, K. Diedkova, A. Roshchupkin, et al., "Development of Hydrophilic NbCuSi(N) &TiAlNb(N) Coatings as a New Strategy for Medical Implants Modification," *Ceramics International* 49, no. 3 (February 2023): 4099–4108, https://doi.org/10.1016/j.ceramint.2022.09.290
38. A. N. Aufa, M. Z. Hassan, Z. Ismail, N. Harun, J. Ren, and M. F. Sadali, "Surface Enhancement of Ti–6Al–4V Fabricated by Selective Laser Melting on Bone-Like Apatite Formation," *Journal of Materials Research and Technology* 19 (2022): 4018–4030, https://doi.org/10.1016/j.jmrt.2022.06.135
39. M. Şahin, F. Ünalan, and I. Mutlu, "Corrosion, Ion Release, and Surface Hardness of Ti-6Al-4V and Cobalt-Chromium Alloys Produced by CAD-CAM Milling and Laser Sintering," 128, no. 3 (September): 529.e1–529.e10, https://doi.org/10.1016/j.prosdent.2022.06.011
40. Y. W. Cui, L.-Y. Chen, P. Qin, R. Li, Q. Zang, J. Peng, L. Zhang, S. Lu, L. Wang, and L.-C. Zhang, "Metastable Pitting Corrosion Behavior of Laser Powder Bed Fusion Produced Ti-6Al-4V in Hank's Solution," *Corrosion Science* 203 (2022): 110333, https://doi.org/10.1016/j.corsci.2022.110333
41. R. Ramos de Oliveira, G. Xavier, R. S. Castro, J. B. Porto, L. U, Santos, M. Terada, and A. A. Couto, "Identificação e quantificação de fases de Ti6Al4V produzido por fusão em leito de pó a laser," in *24 Congresso Brasileiro de Engenharia e Ciência dos Materiais* (Águas de Lindóia, Brazil: Instituto de Pesquisas Energéticas e Nucleares, 2022).